Evaluation of reconstructions of snow/ice melt in Greenland by regional atmospheric climate models using laser altimetry data.

Tyler C. Sutterley[1,1], Isabella Velicogna[1,2], Xavier Fettweis[3], Eric Rignot[1,2], Brice Noël[4] and Michiel van den Broeke[4]

Tyler C. Sutterley, tyler.c.sutterley@nasa.gov

[1]Department of Earth System Science, University of California, Irvine, California, USA.

[2]Jet Propulsion Laboratory, California Institute of Technology, Pasadena, California, USA.

[3]Department of Geography, University of Liège, Liège, Belgium.

[4]Institute for Marine and Atmospheric Research, Utrecht University, Utrecht, Netherlands.

This article has been accepted for publication and undergone full peer review but has not been through the copyediting, typesetting, pagination and proofreading process, which may lead to differences between this version and the Version of Record. Please cite this article as doi: 10.1029/2018GL078645

The surface mass balance (SMB) of the Greenland Ice Sheet critically depend on the intensity of ice/snow melt in its ablation zone, but in-situ data have been too limited to quantify the error of regional climate models. Here, we use 23 years of NASA satellite and airborne laser altimetry from the Airborne Topographic Mapper (ATM), Land, Vegetation and Ice Sensor (LVIS) and Ice, Cloud and land Elevation Satellite (ICESat) to generate time series of elevation change to compare with SMB products from the Regional Atmospheric Climate Model (RACMO2.3p2) and from the Modèle Atmosphérique Régional (MARv3.5.2). For 1994-2016, the results agree at the 15-26% level, with the largest discrepancy in north Greenland. During the cold summer 2015, the RMS discrepancy is 40% in the north, 30% in the southwest, and 18-25% at low elevation. The difference drops to 23% in the southwest and 14% at low elevation during the 2016 warm summer.

Keypoints:

- We assess the accuracy of reconstructed runoff from Regional Climate Models, a dominant control on the Greenland Ice Sheet mass balance.
- Time series of mass changes from 23 years of altimetry and seasonal data indicate that the error in runoff is at the 20% level.
- Airborne laser altimetry provides orders of magnitude more data for regional climate model assessment than available in situ.

1. Introduction

Changes in surface mass balance (SMB) of the Greenland Ice Sheet, which are dominated by snow and ice melt at its surface, constitute more than half of its annual mass loss [*van den Broeke et al.*, 2009; *Velicogna et al.*, 2014; *van den Broeke et al.*, 2017]. In situ observations of SMB are too sparse to provide detailed information about SMB processes, especially in the ablation zone. As a result, we rely on regional atmospheric climate models (RCM) constrained by re-analysis data or alternatively the direct statistical downscaling of reanalysis data to reconstruct the ice sheet SMB [*Noël et al.*, 2016; *Ettema et al.*, 2009; *Fettweis*, 2007; *Wilton et al.*, 2017]. Simplified versions of these models are in turn used to project future ice sheet melt in a warming world and the contribution of Greenland to sea level rise [*Tedesco and Fettweis*, 2012].

SMB output products have been evaluated with sparse measurements from shallow ice cores, in-situ stake sites, and automatic weather stations (AWS) [*Bales et al.*, 2009; *Cogley*, 2004; *Reeh*, 2008; *van de Wal et al.*, 2012]. The agreement between these observations is best in areas of net accumulation compared to areas of net ablation [*Vernon et al.*, 2013]. The agreement is reasonably accurate in the accumulation area, with performance levels typically 9% [*van den Broeke et al.*, 2016]. In the ablation zone, in situ data are few and generally not over extended period of times which makes it challenging to assess model performance [*Noël et al.*, 2017a; *Fettweis et al.*, 2017]. By default, an uncertainty of 20% has been assumed for ice sheet runoff in Greenland, mostly from a comparison with one set of data in southwest Greenland [*Shepherd et al.*, 2012]. This uncertainty limits the

reliability of projections of future changes in ice sheet surface mass balance in a warming climate.

In this study, we analyze 23 years of airborne and satellite laser altimetry collected over Greenland since 1994 to document elevation changes in the ablation zone [*Krabill et al.*, 2004]. These measurements provide a comprehensive assessment of changes in surface mass balance around Greenland once the results are converted into mass changes. In order to obtain reliable, comprehensive, and long time series, we use a triangulated irregular networks (TIN) method that combines measurements from several platforms: 1) the Airborne Topographic Mapper (ATM), 2) the Land, Vegetation and Ice Sensor (LVIS) and 3) the Ice, Cloud and land Elevation Satellite (ICESat). The time series of mass changes are compared with surface mass balance output products from two widely used regional atmospheric climate models: 1) the Regional Atmospheric Climate Model (RACMO2.3p2) and 2) the Modèle Atmosphérique Régional (MARv3.5.2) [*Noël et al.*, 2015; *Fettweis*, 2007]. We focus our analysis on regions within the ablation zone with low ice velocity to minimize the impact of ice dynamics [*Rignot and Mouginot*, 2012]. We quantify the differences across various regions and varying time periods, including summer seasons. We conclude on the precision of SMB reconstructions of snow/ice melt processes in the ablation zone of Greenland.

2. Data and Methods

Laser altimetry. We use Release-33 of the ICESat GLA12 Antarctic and Greenland Ice Sheet Altimetry product provided by NSIDC [*Zwally et al.*, 2014]. As the accuracy of the ICESat elevation measurements is degraded by the presence of clouds, we remove

cloud-affected data points using a set of culling criteria following *Howat et al.* [2008]; *Pritchard et al.* [2009]; *Smith et al.* [2009]; *Sørensen et al.* [2011]. The ICESat elevation measurements are converted to be in reference to the WGS-84 ellipsoid, corrected for saturation effects with the GLA12 correction product [*Zwally et al.*, 2014] and corrected for Gaussian-Centroid (G-C) offset [*Borsa et al.*, 2014]. Our airborne lidar measurements are Level-2 Airborne Topographic Mapper (ATM Icessn) and Land, Vegetation and Ice Sensor (LVIS) datasets provided by NSIDC [*Thomas and Studinger*, 2010; *Studinger*, 2014a; *Blair and Hofton*, 2010]. ATM is a conically scanning lidar developed at the NASA Wallops Flight Facility (WFF) which has flown extensively in Greenland since 1993 [*Krabill*, 2000; *Brunt et al.*, 2017]. LVIS is a large-swath scanning lidar developed at NASA's Goddard Space Flight Center (GSFC) which has flown in Greenland from 2007 to 2013 [*Blair et al.*, 1999; *Hofton et al.*, 2008]. The Level-2 LVIS data supplies 3 different elevation surfaces calculated from the Level-1B full waveform product: the highest and lowest returning surfaces via Gaussian decomposition, and the centroidal surface [*Blair and Hofton*, 2010]. We use the lowest returning surface when the waveform resembles a single-peak gaussian and the centroid surface when the waveform is multi-peak. For most simple, non-complex terrains the high and low surfaces are equivalent and the return waveform is single-peak. Each elevation dataset is converted to be in reference to the 2014 solution of the International Terrestrial Reference Frame (ITRF) [*Altamimi et al.*, 2016]. Rates of crustal uplift due to Glacial Isostatic Adjustment (GIA) are subtracted from the altimetry data following *A et al.* [2013], *Farrell* [1972] and *Wahr et al.* [2000] using coefficients from *Simpson et al.* [2009].

Integrated analysis of altimetry. We calculate rates of elevation change by comparing a set of measured elevation values with a set of interpolated elevations from a different time period. The method follows the altimetry analysis of *Pritchard et al.* [2009] and *Rignot et al.* [2013], with the addition of higher-resolution airborne altimetry datasets. The set of interpolated values are constructed using triangulated irregular networks (TIN) based on Delaunay triangulation [*Pritchard et al.*, 2009, 2012]. For each data point in a flight line, a set of Delaunay triangles is constructed from a separate flight line using all data points within 300 meters from the original point. If the original point lies within the confines of the Delaunay triangulation convex hull, the triangular facet housing the original point is determined using a winding number algorithm, a simple test to find if a point is within a polygon. The new elevation value is calculated using barycentric interpolation with the elevation measurements at the three triangle vertices. In this interpolation scheme, the elevation at each vertex point is weighted by the area of the triangle created by the enclosed point and the two remaining vertices (Figure S1). Assuming that the ice sheet surface is not curved over the scale of the individual triangular facet, interpolating to the original coordinates compensates for slopes in the ice sheet surface. Crevassed terrain, snow drifts, and low-lying clouds contaminate the lidar elevation values for the interpolation. In order to limit the effect of contaminated points, elevation change rates are filtered using an interquartile range algorithm [*Pritchard et al.*, 2009]. In all, we calculate approximately 2 million kilometers of elevation change rates from 1993 to 2016 over the Greenland ice sheet. We reduce our complete dataset to locations where surface

velocities are low (at most 100 m/yr) to avoid contamination from in ice dynamics [*Rignot and Mouginot*, 2012].

Conversion of elevation change to mass change. Our elevation change estimates are converted to mass using the density of ice (ρ_{ice}: 900 kg/m^3), which assumes that the elevation changes are occurring over bare ice, not snow (ρ_{snow}: $100 - 550$ kg/m^3) or firn ice (ρ_{firn}: $550 - 830$ kg/m^3). If a significant snow layer thickness accumulated in the winter, the density at which elevation changes take place may be lower than the density of ice. The regional atmospheric climate models use different ice densities. RACMO2 uses an ice density of 910 kg/m^3 and MAR uses an ice density of 920 kg/m^3. We include this uncertainty in our error estimates. However, the conversion from volume change to mass change is non-trivial and the density assumption is a key source of uncertainty.

Surface Mass Balance output products. SMB is the sum of mass accumulation from snow and rain minus the surface ablation from meltwater runoff, sublimation, and snow drift erosion [*Ettema et al.*, 2009; *Lenaerts et al.*, 2012]. The runoff component is the portion of total snowmelt not retained or refrozen within the firn layer covering the ice sheet. We use monthly mean components of SMB calculated from climate simulations by the Regional Atmospheric Climate Model (RACMO2.3p2, 1958–2016) and Modèle Atmosphérique Régional (MAR 3.5.2, 1958–2015) [*Noël et al.*, 2015; *Fettweis*, 2007].

RACMO2 is a high-resolution (11 km) RCM combining the dynamics of the HIRLAM numerical weather prediction model with the physical processes represented in the European Centre for Medium-Range Weather Forecast (ECMWF) model [*Unden et al.*, 2002; *White*, 2002]. RACMO2.3p2 has updated glacial topography, glacial delineations, and ice

albedo fields as well as improved tuning of cloud, snow property and melt parameterizations [*Noël et al.*, 2017b].

MAR couples a high-resolution (20 km) regional climate model with the Soil Ice Snow Vegetation Atmosphere Transfer (SISVAT) scheme [*Fettweis*, 2007; *Gallée and Schayes*, 1994; *De Ridder and Gallée*, 1998]. The internal snow and ice component of SISVAT is based on the CROCUS snow model [*Brun et al.*, 1992].

For both RACMO2 and MAR, climate forcing is from ERA-40 (1958–1978) and ERA-Interim (1979 onward) reanalysis datasets at the lateral boundaries and at the sea surface on a 6-hour basis. Both models are downscaled using the Greenland Ice Mapping Project (GIMP) digital elevation model provided by the Glacier Dynamics Group at Ohio State University [*Howat et al.*, 2014; *Bamber et al.*, 2013]. The RACMO2 data is statistically downscaled from 11 to 1 km as described in *Noël et al.* [2016] and MAR data is downscaled from 20 km to 5 km following *Franco et al.* [2012]. The downscaling yields higher rates of ice ablation at low elevation and more realistic patterns of SMB in terminal glacial fjords, valleys, and depressions where coarser-resolution original models cannot resolve the local-scale topography [*Noël et al.*, 2016; *Wilton et al.*, 2017].

Cumulative anomalies in SMB and individual SMB components are calculated in reference to a period of near-zero total mass balance, which is 1961 to 1990 [*van den Broeke et al.*, 2009]. During this 30-year reference period, the ice sheet is assumed to have been close to balance [*van den Broeke et al.*, 2009; *Rignot et al.*, 2008]. Uncertainties in cumulative SMB anomalies are calculated considering 10 separate 20-year baselines following *van den Broeke et al.* [2009]. These uncertainties take into account the inhomogeneity

in the RCM forcing with the use of ERA40 for the period before 1979 and ERA-Interim after 1979, and help address the assumption of stability during the 30-year baseline [*Colgan et al.*, 2015]. Nevertheless, the assumption of a stable ice sheet during this 30-year baseline may not be fully accurate at the regional level. Ablation zones for each RCM are delineated using the equilibrium-line altitude (ELA) which is the spatially varying elevation where the mean SMB is zero over a specific time period. We use the ELA for the time period 1993 to 2015 from each RCM to determine the transition altitude for elevation to mass conversion.

We compare the laser altimetry time series of mass changes with the SMB output products from the RCMs at four sites in different parts of Greenland between 1994 and 2016 and during several summer seasons in Southwest and North Greenland for the summer 2015 and in Southwest Greenland for the summer 2016 (the 2016 campaign did not cover the northern part of Greenland due to technical difficulties).

3. Results

Validation of the TIN method. We compare elevation changes from the TIN method with the Pre-IceBridge and Operation IceBridge ATM Level-4 Surface Elevation Rate of Change product (idhdt) provided by NSIDC [*Studinger*, 2014b]. The Level-4 elevation change product computes rates directly from the Level-1B Qfit elevation products [*Studinger*, 2013]. To compare the two methods, we rasterize the estimates of elevation change rates from both techniques into 5 km by 5 km polar stereographic grids. We then compare the spatial patterns and average elevation differences between the two techniques. For the high melt years covering Spring 2011 to Spring 2013 and the high accumulation

season covering Spring 2013 to Spring 2014, the results demonstrate that the TIN method produces coherent measurements of surface elevation change (Figure S2). The addition of LVIS data increases the spatial coverage of the elevation measurements, most significantly in southwest Greenland for the 2011–2013 period. The agreement between ATM and LVIS for near concurrent acquisitions (less than 10 days apart) is 24 cm, which certifies that the two lidars are compatible and complementary. The cell-for-cell RMS difference between the idhdt product and the TIN method is 68 cm, which is less than the combined average error of both datasets (109 cm). Most of the differences and sources of error are found in regions with high surface roughness where the derivation of elevation change from laser altimetry is not a trivial task [*Krabill et al.*, 1999]. Over most regions, the TIN change rates are smoother than the idhdt product.

Evaluation of RCM on decadal time scales. We compare the altimetry time series with RACMO2 and MAR at four other locations on the ice sheet using nearly continuous time series between 1994 and 2016: 1) Site-5 of the University of Utrecht K-transect in West Greenland from *van de Wal et al.* [2012] (Figures 1a, S7), 2) PROMICE Kronprins Christian (KPC) AWS in Northeast Greenland (or NE Promice Lower, Figures 1b, S8), 3) land-terminating Saqqap Sermersua in Southwest Greenland (Figures 1d, S9) and 4) inland of Hiawatha glacier in North Greenland (Figures 1e, S10). These locations maximize the number of elevation points available, minimize the impact of flow speed (speed less than 30 m/yr with no known change in speed), and include measurements from the Fall 2015 campaign for the K-transect and Hiawatha glacier sites.

At the K-transect (Figure 1a), the altimetry data shows a period of relative stability in elevation in the 1990's that is not apparent in the SMB data. The increase in thinning after 2002 is however well captured by both models. The RMS difference between our altimetry estimates and RCMs for each measurement and the percent difference with reference to the SMB change is 4070±1740 mm w.e. (25%) and 1560±1010 (18%) for MAR and RACMO2, respectively. After 1999, the RMS difference improves to 2960±1740 mm w.e. (20%) and 1330±980 (15%) for MAR and RACMO2, respectively. At the NE PROMICE Lower site (Figure 1b), both models are similar but overestimate the mass change compared to altimetry by 1330±160 mm w.e. (25%) and 1410±450 (25%) for MAR and RACMO2, respectively. At the Saqqap Sermersua site (Figure 1c), the RMS difference is 1330±1050 mm w.e. (11%) and 1650±1300 (19%), respectively. At the Hiawatha glacier site (Figure 1d), MAR does better in terms of long term changes with a RMS of 180±120 mm w.e. (7%) versus 570±160 (15%) for RACMO2.

Evaluation of RCM over summer seasons. We compare altimetry data collected in spring and fall of 2015 and 2016 to capture the summer melt in Southwest and North Greenland (Figure 2). In the Southwest, we use 690 km of data from 2015 and 530 km of data from 2016, ranging from the ice divide in the north to 65°N in the south, with all data below the ELA. In North Greenland, we use 130 km of data from 2015, below the ELA [*Rignot and Mouginot*, 2012]. We calculate the mass changes and RMS differences over 50 m elevation bands, above and below 1,000 m elevation, and for the entire range of elevation (Table 1). In the Southwest, the agreement is at the 20–60% level with RACMO2 and 40–54% level with MAR in 2015. Above 1,000 m, RACMO2 is within 53%

and MAR within 47%. In 2016, the agreement is at the 9–39% level with RACMO2 in the Southwest. Below 1,000 m, RACMO2 agrees with altimetry within 14% and within 30% above 1,000m. MARv3.5.2 is the last version with consistent forcing from ERA40 and ERA-Interim that covers the full 1961–1990 reference period. However, MARv3.5.2 outputs are not available for the 2016 season. In the North, the agreement with RACMO2 ranges from 19 to 42% versus 18 to 44% for MAR. The RCMs agree within 25–30% at low elevation and 38 to 40% at high elevation, with an overall error in total mass change of 30–35%.

4. Discussion

Our integration of multiple laser altimetry datasets into a single, comprehensive record significantly increases the total spatial coverage of elevation measurements in Greenland compared to any single instrument. The time series of measurements provides orders of magnitude more points of evaluation of the RCMs than available from in situ data. The TIN method yields coherent estimates of surface elevation change, at a high spatial resolution (10–50 m), ten times better than the 500 m rasterization of *Kjeldsen et al.* [2013] and *Khan et al.* [2014]. Our approach calculates elevation change on a shot-by-shot basis, which is different from the surface fit method of *Schenk and Csatho* [2012] that simultaneously solves for surface elevation change and surface slope over kilometer-scale surface patches.

Differences between altimetry and RCMs reflect errors in the altimetry data, RCM output products, and in the density conversion from elevation to mass change. These errors vary spatially and temporarily. To diagnose the origin of the differences between

altimetry and models, it is useful to compare the model components. In terms of accumulation, we find only small differences in precipitation between RACMO and MAR at the four sites (Figures S3 and S11). At the K-transect, we find a 47% difference between RACMO2.3p2 and MARv3.5.2 (Figure S4) which, if we use the altimetry data as a benchmark, is mostly due to snowmelt being overestimated by MARv3.5.2. Conversely, at the Hiawatha Gletscher site, RACMO2.3p2 produces 28% less runoff than MARv3.5.2, MARv3.5.2 produces more snowmelt but a greater fraction is retained as melt refreeze, yielding a better agreement with altimetry. In the Southwest or NE Greenland, the differences between the model components are smaller, yet both models seem to overestimate melt.

There are a number of differences between MAR and RACMO2 that make the comparison difficult. Runoff is a function of surface slope in MAR while meltwater runs off directly after saturating the firn layer in RACMO2. The two models use different bare ice albedo which may explain why runoff is higher in MAR for sites in Figure 1a and 1c compared to RACMO. The snow models are different and despite the agreement in total precipitation, the ELAs are different, especially in the northeast. At the current level of difference between the two models and the altimetry data, it is challenging to determine which model component requires improvement. Our results do not provide definite trends due to uncertainties in the density conversion of altimetry data and the differences vary by region, with larger errors in the north. The work here highlights the need for more systematic comparisons between the models quantifying Greenland SMB, such as a Model Intercomparison Project (MIP) and the work of *Vernon et al.* [2013], in order

to diagnose the regional differences. Finer time series capable of documenting individual snowfall events and melt events are likely necessary to help refine the assessment and model diagnosis. The upcoming ICESat-2 mission may be able to help rectify some of these challenges by providing data at seasonal time-scales over the entirety of the ice sheet [*Markus et al.*, 2017].

In general, we find that both RCM models track the long term trends in SMB remarkably well (Figure 1), especially in high melt regions, such as in the Southwest, where the difference between altimetry and RCMs is at the 11–26% level. Over a single summer season, the percentage error increases, as expected. The melt-season in 2015 was below-average in Southwest Greenland and above-average in North Greenland [*Blunden and Arndt*, 2016; *Tedesco et al.*, 2016]. Southwest Greenland in 2016 was warm and the melt-season was stronger than average with large swaths of bare ice exposed [*Blunden and Arndt*, 2017]. In the warm summer of 2016, RACMO2 model performance is excellent and superior to 2015. The lower performance in 2015 may indicate issues with underestimated snow thickness at the end of the winter season.

Overall, for large areas and over long time periods, the RCMs reconstruct runoff with an accuracy of about 20%. At the regional level, the error may range anywhere from 14% to 40%. The larger uncertainties in the north affect local assessments but have a low impact on total runoff from Greenland because runoff is low in north Greenland (Figure S4).

With the launch of ICESat-2, the time series will extend in time and especially vastly improve in terms of revisit frequency [*Abdalati et al.*, 2010; *Markus et al.*, 2017]. The

mission will operate with a 91 day repeat instead of annual to sub-annual with OIB. The near repeat subcycle will be 1 month and some crossover areas near the poles will be revisited on a daily basis. This temporal resolution will vastly improve the diagnosis of the limitations of RCMs and provide more definite guidelines on how to improve RCMs.

5. Conclusions

We present a methodology for evaluating SMB outputs from RCMs in the ablation zone of Greenland that spans multiple decades, from seasonal to multi-annual, along 10,000's km of data. We find that the SMB products from the RACMO2 and MAR regional atmospheric climate models have a remarkable accuracy at the 15–26% level over the long term, hence capturing long term trends in SMB in the ablation zone of Greenland with reasonable accuracy. We caution that the model error increases during cold periods and varies significantly spatially, with larger errors in in the north compared to Southwest. Differences in snow thickness and meltwater refreezing probably explain the majority of the differences between the models and with the altimetry data, but more data ought to be acquired over shorter time intervals to provide more definite guidance for RCM improvement.

Acknowledgments. This work was performed at UC Irvine and JPL-Caltech funded by grants from the NASA's Cryosphere, Terrestrial Hydrology, Interdisciplinary Science, and MEASURES-2 Programs, Contracts JPL-1390432, UTA12-000609 and UTA13-000917. Data used here are available on our website (https://www.ess.uci.edu/~velicogna/data.html) and will be archived at NSIDC. Computations were performed on the UC Irvine Greenplanet High Performance Computing

Cluster. We thank the NASA Operation IceBridge flight, instrument and science teams for collecting and producing the science data, the editor and anonymous reviewers for their comments, and Jeremie Mouginot (UC Irvine) for his advice on the laser altimetry analysis.

Notes

1. Now at NASA Goddard Space Flight Center, Greenbelt, Maryland, USA.

2. Now at NASA Goddard Space Flight Center, Greenbelt, Maryland, USA.

References

A, G., J. Wahr, and S. Zhong (2013), Computations of the viscoelastic response of a 3-D compressible Earth to surface loading: an application to Glacial Isostatic Adjustment in Antarctica and Canada, *Geophysical Journal International*, *192*(2), 557–572, doi: 10.1093/gji/ggs030.

Abdalati, W., H. J. Zwally, R. Bindschadler, B. M. Csatho, S. L. Farrell, H. A. Fricker, D. Harding, R. Kwok, M. Lefsky, T. Markus, A. Marshak, T. A. Neumann, S. P. Palm, B. E. Schutz, B. E. Smith, J. Spinhirne, and C. Webb (2010), The ICESat-2 Laser Altimetry Mission, *Proceedings of the IEEE*, *98*(5), 735–751, doi: 10.1109/JPROC.2009.2034765.

Altamimi, Z., P. Rebischung, L. Métivier, and X. Collilieux (2016), ITRF2014: A new release of the International Terrestrial Reference Frame modeling nonlinear station motions, *Journal of Geophysical Research: Solid Earth*, *121*(8), 6109–6131, doi: 10.1002/2016JB013098, 2016JB013098.

Bales, R. C., Q. Guo, D. Shen, J. R. McConnell, G. Du, J. F. Burkhart, V. B. Spikes, E. Hanna, and J. Cappelen (2009), Annual accumulation for Greenland updated using ice core data developed during 2000–2006 and analysis of daily coastal meteorological data, *Journal of Geophysical Research: Atmospheres*, *114*(D6), doi: 10.1029/2008JD011208, d06116.

Bamber, J. L., J. A. Griggs, R. T. W. L. Hurkmans, J. A. Dowdeswell, S. P. Gogineni, I. M. Howat, J. Mouginot, J. D. Paden, S. Palmer, E. J. Rignot, and D. Steinhage (2013), A new bed elevation dataset for Greenland, *The Cryosphere*, *7*(2), 499–510, doi:10.5194/tc-7-499-2013.

Blair, J. B., and M. Hofton (2010), *IceBridge LVIS L2 Geolocated Surface Elevation Product*, NASA DAAC at the National Snow and Ice Data Center, Boulder, Colorado USA, version 2.

Blair, J. B., D. L. Rabine, and M. A. Hofton (1999), The Laser Vegetation Imaging Sensor: a medium-altitude, digitisation-only, airborne laser altimeter for mapping vegetation and topography, *ISPRS Journal of Photogrammetry and Remote Sensing*, *54*(2-3), 115–122, doi:10.1016/S0924-2716(99)00002-7.

Blunden, J., and D. S. Arndt (2016), State of the Climate in 2015, *Bulletin of the American Meteorological Society*, *97*(8), 275, doi:10.1175/2016BAMSStateoftheClimate.1.

Blunden, J., and D. S. Arndt (2017), State of the Climate in 2016, *Bulletin of the American Meteorological Society*, *98*(8), 280, doi:10.1175/2017BAMSStateoftheClimate.1.

Borsa, A. A., G. Moholdt, H. A. Fricker, and K. M. Brunt (2014), A range correction for ICESat and its potential impact on ice-sheet mass balance studies, *The Cryosphere*,

8(2), 345–357, doi:10.5194/tc-8-345-2014.

Brun, E., P. David, M. Sudul, and G. Brunot (1992), A numerical model to simulate snow-cover stratigraphy for operational avalanche forecasting, *Journal of Glaciology*, *38*(128), 13–22, doi:10.1017/S0022143000009552.

Brunt, K. M., R. L. Hawley, E. R. Lutz, M. Studinger, J. G. Sonntag, M. A. Hofton, L. C. Andrews, and T. A. Neumann (2017), Assessment of NASA airborne laser altimetry data using ground-based GPS data near Summit Station, Greenland, *The Cryosphere*, *11*(2), 681–692, doi:10.5194/tc-11-681-2017.

Cogley, J. G. (2004), Greenland accumulation: An error model, *Journal of Geophysical Research: Atmospheres*, *109*(D18), doi:10.1029/2003JD004449, d18101.

Colgan, W., J. E. Box, M. L. Andersen, X. Fettweis, B. M. Csatho, R. S. Fausto, D. van As, and J. Wahr (2015), Greenland high-elevation mass balance: inference and implication of reference period (1961–90) imbalance, *Annals of Glaciology*, *56*(70), 105–117, doi:10.3189/2015AoG70A967.

De Ridder, K., and H. Gallée (1998), Land Surface–Induced Regional Climate Change in Southern Israel, *Journal of Applied Meteorology*, *37*(11), 1470–1485, doi:10.1175/1520-0450(1998)037¡1470:LSIRCC¿2.0.CO;2.

Ettema, J., M. R. van den Broeke, E. van Meijgaard, W. J. van de Berg, J. L. Bamber, J. E. Box, and R. C. Bales (2009), Higher surface mass balance of the Greenland ice sheet revealed by high-resolution climate modeling, *Geophysical Research Letters*, *36*(12), doi:10.1029/2009GL038110, l12501.

Farrell, W. E. (1972), Deformation of the Earth by surface loads, *Reviews of Geophysics*, *10*(3), 761–797, doi:10.1029/RG010i003p00761.

Fettweis, X. (2007), Reconstruction of the 1979–2006 Greenland ice sheet surface mass balance using the regional climate model MAR, *The Cryosphere*, *1*(1), 21–40, doi:10.5194/tc-1-21-2007.

Fettweis, X., J. E. Box, C. Agosta, C. Amory, C. Kittel, C. Lang, D. van As, H. Machguth, and H. Gallée (2017), Reconstructions of the 1900–2015 Greenland ice sheet surface mass balance using the regional climate MAR model, *The Cryosphere*, *11*(2), 1015–1033, doi:10.5194/tc-11-1015-2017.

Franco, B., X. Fettweis, C. Lang, and M. Erpicum (2012), Impact of spatial resolution on the modelling of the Greenland ice sheet surface mass balance between 1990–2010, using the regional climate model MAR, *The Cryosphere*, *6*(3), 695–711, doi:10.5194/tc-6-695-2012.

Gallée, H., and G. Schayes (1994), Development of a Three-Dimensional Meso-γ Primitive Equation Model: Katabatic Winds Simulation in the Area of Terra Nova Bay, Antarctica, *Monthly Weather Review*, *122*(4), 671–685, doi:10.1175/1520-0493(1994)122¡0671:DOATDM¿2.0.CO;2.

Hofton, M. A., J. B. Blair, S. B. Luthcke, and D. L. Rabine (2008), Assessing the performance of 20–25 m footprint waveform lidar data collected in ICESat data corridors in Greenland, *Geophysical Research Letters*, *35*(24), doi:10.1029/2008GL035774, l24501.

Howat, I. M., B. E. Smith, I. R. Joughin, and T. A. Scambos (2008), Rates of southeast Greenland ice volume loss from combined ICESat and ASTER observations, *Geophysical*

Research Letters, *35*(17), doi:10.1029/2008GL034496, l17505.

Howat, I. M., A. Negrete, and B. E. Smith (2014), The Greenland Ice Mapping Project (GIMP) land classification and surface elevation data sets, *The Cryosphere*, *8*(4), 1509–1518, doi:10.5194/tc-8-1509-2014.

Khan, S. A., K. H. Kjær, M. Bevis, J. L. Bamber, J. Wahr, K. K. Kjeldsen, A. A. Bjørk, N. J. Korsgaard, L. A. Stearns, M. R. van den Broeke, L. Liu, N. K. Larsen, and I. S. Muresan (2014), Sustained mass loss of the northeast Greenland ice sheet triggered by regional warming, *Nature Climate Change*, *4*(4), 292–299, doi:10.1038/nclimate2161.

Kjeldsen, K. K., S. A. Khan, J. Wahr, N. J. Korsgaard, K. H. Kjær, A. A. Bjørk, R. Hurkmans, M. R. van den Broeke, J. L. Bamber, and J. H. van Angelen (2013), Improved ice loss estimate of the northwestern Greenland ice sheet, *Journal of Geophysical Research: Solid Earth*, *118*(2), 698–708, doi:10.1029/2012JB009684.

Krabill, W. B. (2000), Greenland Ice Sheet: High-Elevation Balance and Peripheral Thinning, *Science*, *289*(5478), 428–430, doi:10.1126/science.289.5478.428.

Krabill, W. B., E. B. Frederick, S. S. Manizade, C. F. Martin, J. G. Sonntag, R. N. Swift, R. H. Thomas, W. Wright, and J. G. Yungel (1999), Rapid Thinning of Parts of the Southern Greenland Ice Sheet, *Science*, *283*(5407), 1522–1524, doi:10.1126/science.283.5407.1522.

Krabill, W. B., E. Hanna, P. Huybrechts, W. Abdalati, J. Cappelen, B. M. Csatho, E. B. Frederick, S. S. Manizade, C. F. Martin, J. G. Sonntag, R. N. Swift, R. H. Thomas, and J. G. Yungel (2004), Greenland Ice Sheet: Increased coastal thinning, *Geophysical Research Letters*, *31*(24), doi:10.1029/2004GL021533, l24402.

Lenaerts, J. T. M., M. R. van den Broeke, W. J. van de Berg, E. van Meijgaard, and P. Kuipers Munneke (2012), A new, high-resolution surface mass balance map of Antarctica (1979–2010) based on regional atmospheric climate modeling, *Geophysical Research Letters*, *39*(4), doi:10.1029/2011GL050713, l04501.

Markus, T., T. Neumann, A. Martino, W. Abdalati, K. Brunt, B. Csatho, S. Farrell, H. Fricker, A. Gardner, D. Harding, M. Jasinski, R. Kwok, L. Magruder, D. Lubin, S. Luthcke, J. Morison, R. Nelson, A. Neuenschwander, S. Palm, S. Popescu, C. Shum, B. E. Schutz, B. Smith, Y. Yang, and J. Zwally (2017), The Ice, Cloud, and land Elevation Satellite-2 (ICESat-2): Science requirements, concept, and implementation, *Remote Sensing of Environment*, *190*, 260–273, doi:10.1016/j.rse.2016.12.029.

Noël, B., W. J. van de Berg, E. van Meijgaard, P. Kuipers Munneke, R. S. W. van de Wal, and M. R. van den Broeke (2015), Evaluation of the updated regional climate model RACMO2.3: summer snowfall impact on the Greenland Ice Sheet, *The Cryosphere*, *9*(5), 1831–1844, doi:10.5194/tc-9-1831-2015.

Noël, B., W. J. van de Berg, H. Machguth, S. Lhermitte, I. M. Howat, X. Fettweis, and M. R. van den Broeke (2016), A daily, 1 km resolution data set of downscaled Greenland ice sheet surface mass balance (1958–2015), *The Cryosphere*, *10*(5), 2361–2377, doi:10.5194/tc-10-2361-2016.

Noël, B., W. J. van de Berg, S. Lhermitte, B. Wouters, H. Machguth, I. Howat, M. Citterio, G. Moholdt, J. T. M. Lenaerts, and M. R. van den Broeke (2017a), A tipping point in refreezing accelerates mass loss of Greenland?s glaciers and ice caps, *Nature Communications*, *8*, 14,730–0, doi:10.1038/ncomms14730.

Noël, B., W. J. van de Berg, J. M. van Wessem, E. van Meijgaard, D. van As, J. T. M. Lenaerts, S. Lhermitte, P. Kuipers Munneke, C. J. P. P. Smeets, L. H. van Ulft, R. S. W. van de Wal, and M. R. van den Broeke (2017b), Modelling the climate and surface mass balance of, *The Cryosphere Discussions*, *2017*, 1–35, doi:10.5194/tc-2017-201.

Pritchard, H. D., R. J. Arthern, D. G. Vaughan, and L. A. Edwards (2009), Extensive dynamic thinning on the margins of the Greenland and Antarctic ice sheets, *Nature*, *461*(7266), 971–975, doi:10.1038/nature08471.

Pritchard, H. D., S. R. M. Ligtenberg, H. A. Fricker, D. G. Vaughan, M. R. van den Broeke, and L. Padman (2012), Antarctic ice-sheet loss driven by basal melting of ice shelves, *Nature*, *484*(7395), 502–505, doi:10.1038/nature10968.

Reeh, N. (2008), A nonsteady-state firn-densification model for the percolation zone of a glacier, *Journal of Geophysical Research: Earth Surface*, *113*(F3), doi:10.1029/2007JF000746, f03023.

Rignot, E. J., and J. Mouginot (2012), Ice flow in Greenland for the International Polar Year 2008–2009, *Geophysical Research Letters*, *39*(11), doi:10.1029/2012GL051634, l11501.

Rignot, E. J., J. E. Box, E. W. Burgess, and E. Hanna (2008), Mass balance of the Greenland ice sheet from 1958 to 2007, *Geophysical Research Letters*, *35*(20), doi:10.1029/2008GL035417, l20502.

Rignot, E. J., S. Jacobs, J. Mouginot, and B. Scheuchl (2013), Ice-shelf melting around antarctica, *Science*, *341*(6143), 266–270, doi:10.1126/science.1235798.

Schenk, T., and B. M. Csatho (2012), A New Methodology for Detecting Ice Sheet Surface Elevation Changes From Laser Altimetry Data, *IEEE Transactions on Geoscience and Remote Sensing*, *50*(9), 3302–3316, doi:10.1109/TGRS.2011.2182357.

Shepherd, A., E. R. Ivins, G. A, V. R. Barletta, M. J. Bentley, S. Bettadpur, K. H. Briggs, D. H. Bromwich, R. Forsberg, N. Galin, M. Horwath, S. Jacobs, I. R. Joughin, M. A. King, J. T. M. Lenaerts, J. Li, S. R. M. Ligtenberg, A. Luckman, S. B. Luthcke, M. McMillan, R. Meister, G. A. Milne, J. Mouginot, A. Muir, J. P. Nicolas, J. D. Paden, A. J. Payne, H. D. Pritchard, E. J. Rignot, H. Rott, L. S. Sørensen, T. A. Scambos, B. Scheuchl, E. Schrama, B. E. Smith, A. V. Sundal, J. H. van Angelen, W. J. van de Berg, M. R. van den Broeke, D. G. Vaughan, I. Velicogna, J. Wahr, P. L. Whitehouse, D. Wingham, D. Yi, D. A. Young, and H. J. Zwally (2012), A Reconciled Estimate of Ice-Sheet Mass Balance, *Science*, *338*(6111), 1183–1189, doi:10.1126/science.1228102.

Simpson, M. J. R., G. A. Milne, P. Huybrechts, and A. J. Long (2009), Calibrating a glaciological model of the Greenland ice sheet from the Last Glacial Maximum to present-day using field observations of relative sea level and ice extent, *Quaternary Science Reviews*, *28*(17-18), 1631–1657, doi:10.1016/j.quascirev.2009.03.004.

Smith, B. E., H. A. Fricker, I. R. Joughin, and S. Tulaczyk (2009), An inventory of active subglacial lakes in Antarctica detected by ICESat (2003–2008), *Journal of Glaciology*, *55*(192), 573–595, doi:10.3189/002214309789470879.

Sørensen, L. S., S. B. Simonsen, K. Nielsen, P. Lucas-Picher, G. Spada, G. Aðalgeirsdottir, R. Forsberg, and C. S. Hvidberg (2011), Mass balance of the Greenland ice sheet (2003–2008) from ICESat data – the impact of interpolation, sampling and firn density, *The*

Cryosphere, *5*(1), 173–186, doi:10.5194/tc-5-173-2011.

Studinger, M. S. (2013), *IceBridge ATM L1B Elevation and Return Strength*, NASA National Snow and Ice Data Center Distributed Active Archive Center, Boulder, Colorado USA, doi:10.5067/19SIM5TXKPGT, version 2.

Studinger, M. S. (2014a), *IceBridge ATM L2 Icessn Elevation, Slope, and Roughness*, NASA National Snow and Ice Data Center Distributed Active Archive Center, Boulder, Colorado USA, doi:10.5067/CPRXXK3F39RV, version 2.

Studinger, M. S. (2014b), *IceBridge ATM L4 Surface Elevation Rate of Change*, NASA National Snow and Ice Data Center Distributed Active Archive Center, Boulder, Colorado USA, doi:10.5067/BCW6CI3TXOCY, version 1.

Tedesco, M., and X. Fettweis (2012), 21st century projections of surface mass balance changes for major drainage systems of the Greenland ice sheet, *Environmental Research Letters*, *7*(4), 045,405, doi:10.1088/1748-9326/7/4/045405.

Tedesco, M., T. Mote, X. Fettweis, E. Hanna, J. Jeyaratnam, J. F. Booth, R. Datta, and K. Briggs (2016), Arctic cut-off high drives the poleward shift of a new Greenland melting record, *Nature Communications*, *7*, 11,723, doi:10.1038/ncomms11723.

Thomas, R. H., and M. S. Studinger (2010), *Pre-IceBridge ATM L2 Icessn Elevation, Slope, and Roughness*, NASA National Snow and Ice Data Center Distributed Active Archive Center, Boulder, Colorado USA, doi:10.5067/6C6WA3R918HJ, version 1.

Unden, P., L. Rontu, H. Järvinen, P. Lynch, J. Calvo, G. Cats, J. Cuxart, K. Eerola, C. Fortelius, and J. A. Garcia-Moya (2002), *HIRLAM-5 scientific documentation*, Swedish Meteorological and Hydrological Institute (SMHI), S-601 76 Norrköping, Swe-

den.

van de Wal, R. S. W., W. Boot, C. J. P. P. Smeets, H. Snellen, M. R. van den Broeke, and J. Oerlemans (2012), Twenty-one years of mass balance observations along the K-transect, West Greenland, *Earth System Science Data*, *4*(1), 31–35, doi:10.5194/essd-4-31-2012.

van den Broeke, M., J. Box, X. Fettweis, E. Hanna, B. Noël, M. Tedesco, D. van As, W. J. van de Berg, and L. van Kampenhout (2017), Greenland Ice Sheet Surface Mass Loss: Recent Developments in Observation and Modeling, *Current Climate Change Reports*, *3*(4), 345–356, doi:10.1007/s40641-017-0084-8.

van den Broeke, M. R., J. L. Bamber, J. Ettema, E. J. Rignot, E. Schrama, W. J. van de Berg, E. van Meijgaard, I. Velicogna, and B. Wouters (2009), Partitioning Recent Greenland Mass Loss, *Science*, *326*(5955), 984–986, doi:10.1126/science.1178176.

van den Broeke, M. R., E. M. Enderlin, I. M. Howat, P. Kuipers Munneke, B. P. Y. Noël, W. J. van de Berg, E. van Meijgaard, and B. Wouters (2016), On the recent contribution of the Greenland ice sheet to sea level change, *The Cryosphere*, *10*(5), 1933–1946, doi:10.5194/tc-10-1933-2016.

Velicogna, I. (2009), Increasing rates of ice mass loss from the Greenland and Antarctic ice sheets revealed by GRACE, *Geophysical Research Letters*, *36*(19), doi:10.1029/2009GL040222, l19503.

Velicogna, I., T. C. Sutterley, and M. R. van den Broeke (2014), Regional acceleration in ice mass loss from Greenland and Antarctica using GRACE time-variable gravity data, *Geophysical Research Letters*, *41*(22), 8130–8137, doi:10.1002/2014GL061052.

Vernon, C. L., J. L. Bamber, J. E. Box, M. R. van den Broeke, X. Fettweis, E. Hanna, and P. Huybrechts (2013), Surface mass balance model intercomparison for the Greenland ice sheet, *The Cryosphere*, *7*(2), 599–614, doi:10.5194/tc-7-599-2013.

Wahr, J., D. Wingham, and C. Bentley (2000), A method of combining ICESat and GRACE satellite data to constrain Antarctic mass balance, *Journal of Geophysical Research: Solid Earth*, *105*(B7), 16,279–16,294, doi:10.1029/2000JB900113.

White, P. W. (2002), *PART IV: PHYSICAL PROCESSES (CY23R4)*, European Centre for Medium-Range Weather Forecasts (ECMWF), Shinfield Park, Reading, RG2 9AX, England.

Wilton, D. J., A. Jowett, E. Hanna, G. R. Bigg, M. R. van den Broeke, X. Fettweis, and P. Huybrechts (2017), High resolution (1 km) positive degree-day modelling of Greenland ice sheet surface mass balance, 1870?2012 using reanalysis data, *Journal of Glaciology*, *63*(237), 176–193, doi:10.1017/jog.2016.133.

Zwally, H. J., R. Schutz, D. Hancock, and J. Dimarzio (2014), *GLAS/ICESat L2 Antarctic and Greenland Ice Sheet Altimetry Data (HDF5)*, NASA National Snow and Ice Data Center Distributed Active Archive Center, Boulder, Colorado USA, doi: 10.5067/ICESAT/GLAS/DATA205, GLA12 Version 34.

Table 1. Comparison of mass change at different elevation bands from Operation IceBridge (OIB) laser altimetry, RACMO2.3p2 and MARv3.5.2 surface mass balance for the 2015 summer season in Southwest Greenland (top three rows) and North Greenland (bottom three rows). OIB data combines elevation measurements from April 18, 2015 and 7 days in October 2015 for Southwest and May 5, 2015 and 4 days in September and October 2015 for North Greenland. Areas of each elevation band are calculated using the Greenland Ice Mapping Project (GIMP) digital elevation model [*Howat et al.*, 2014].

Region	Elevation (m)	IceBridge (mm)	RACMO2 (mm)	MAR (mm)	Area (km^2)	Points
Southwest	519 – 1000	-1200 ± 80	-1530 ± 100	-860 ± 80	9953	1636
	1000 – 1398	-380 ± 60	-460 ± 60	-500 ± 60	31802	4931
	519 – 1398	-570 ± 70	-720 ± 70	-590 ± 70	41755	6567
North	415 – 1000	-750 ± 40	-1040 ± 30	-920 ± 40	2349	4242
	1000 – 1269	-380 ± 20	-630 ± 10	-580 ± 10	2542	3254
	415 – 1269	-560 ± 30	-830 ± 20	-750 ± 30	4891	7496

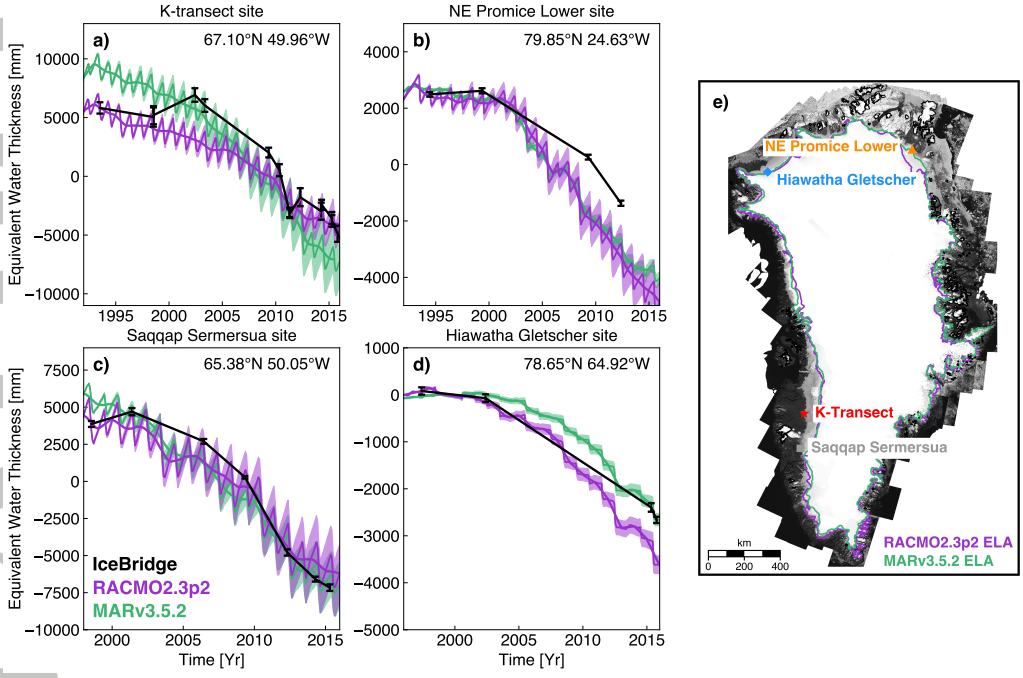

Figure 1. Comparisons of Operation IceBridge (OIB) laser altimetry (black), RACMO2.3p2 surface mass balance (SMB) (purple) and MARv3.5.2 SMB (green) at a) Site 5 of the K-transect in West Greenland, b) NE Promice Lower in Northeast Greenland, c) Saqqap Sermersua in Southwest Greenland, and d) Hiawatha Gletscher in North Greenland. Thick purple and green lines are the 13-month smoothed SMB time series [*Velicogna*, 2009]. e) Locations of the K-transect (red star), NE Promice Lower (orange triangle), Saqqap Sermersua (gray square), Hiawatha Gletscher (blue diamond) sites. Purple and green lines denote the ELA from each model. Overlaid on an image mosaic from the Greenland Ice Mapping Project [*Howat et al.*, 2014].

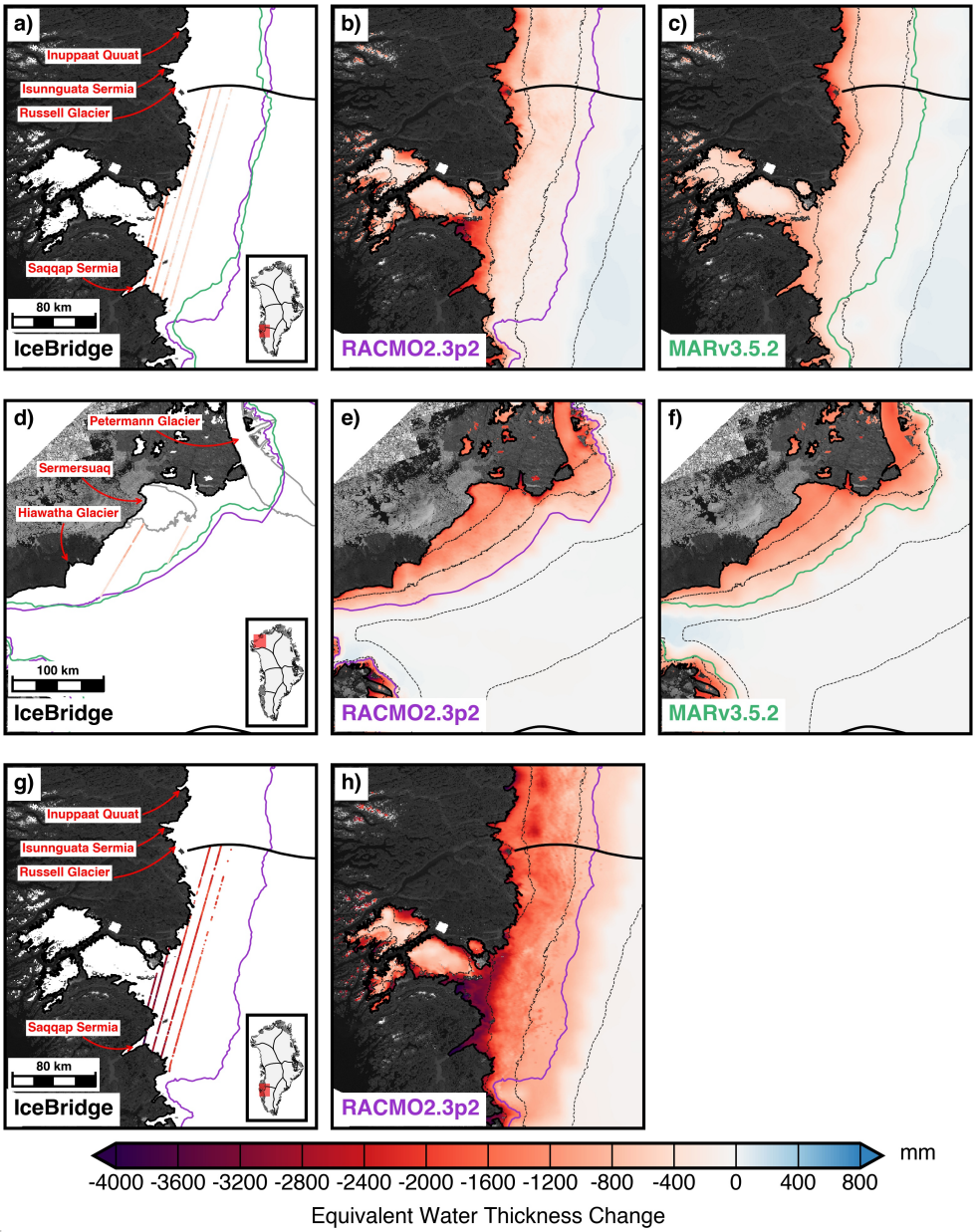

Figure 2. Comparisons of mass change from a,d,g) Operation IceBridge (OIB) laser altimetry, b,e,h) RACMO2.3p2 surface mass balance (SMB) and c,f) MARv3.5.2 SMB over the 2015 summer season for (a-c) Southwest Greenland and (d-f) North Greenland and over the 2016 summer season for (g-h) Southwest Greenland. OIB combines data from April 18, 2015 with data collected during 7 days in October 2015 for (a-c), data from May 5, 2015 and 2 days in October 2015 for (d-f) and data from May 14, 2016 with data collected during 6 days in August and September 2016 for (g-h). SMB outputs from MARv3.5.2 are not available for 2016. Purple and green lines are the ELA positions from RACMO2 and MAR, respectively, for the period 1993–2015. Gray lines in d) denote the 100 m/yr ice speed contour from *Rignot and Mouginot* [2012]. Thick black lines denote ice divides from *Rignot and Mouginot* [2012]. Dashed lines denote 500 m elevation contours from the Greenland Ice Mapping Project (GIMP) [*Howat et al.*, 2014]. Inset map denotes the location of the maps.

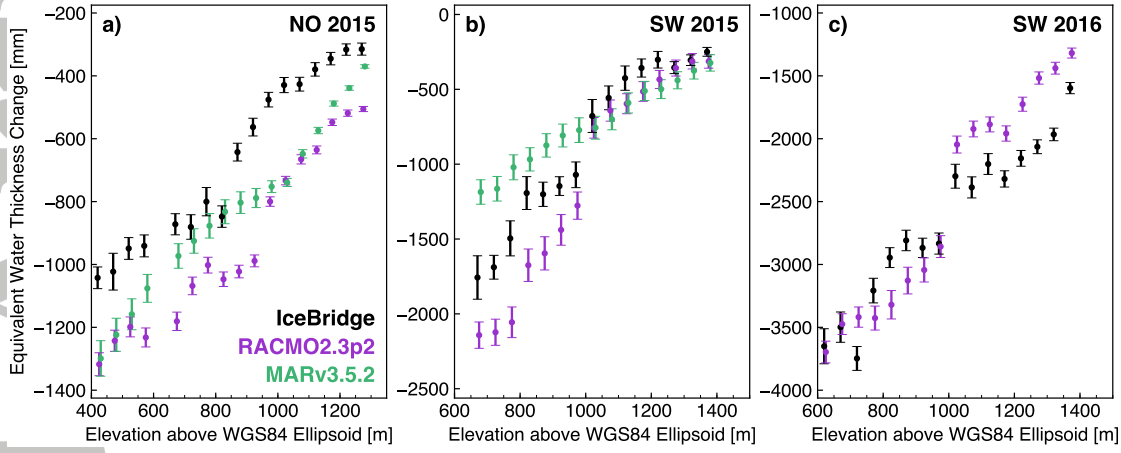

Figure 3. Comparison of mass change at different elevation bands from Operation IceBridge (OIB) laser altimetry (black), RACMO2.3p2 surface mass balance (SMB) (purple) and MARv3.5.2 SMB (green) over the summer seasons from a) 2015 in North Greenland (Figure 2d-f), b) 2015 in Southwest Greenland (Figure 2a-c) and c) 2016 in Southwest Greenland (Figure 2g-h).